Macromolecules

ARTICLE

pubs.acs.org/Macromolecules

Analyte-Reactive Amphiphilic Thermoresponsive Diblock Copolymer Micelles-Based Multifunctional Ratiometric Fluorescent Chemosensors

Jinming Hu, Lu Dai, and Shiyong Liu*

CAS Key Laboratory of Soft Matter Chemistry, Department of Polymer Science and Engineering, Hefei National Laboratory for Physical Sciences at the Microscale, University of Science and Technology of China, Hefei, Anhui 230026, China

Supporting Information

ABSTRACT: We report on the fabrication of amphiphilic thermoresponsive diblock copolymer micelle-based multifunctional ratiometric fluorescent chemosensors for metal ions (Hg^{2+} and Cu^{2+}), pH, and temperatures. A fluorescence resonance energy transfer (FRET) pair consisting of 4-(2-acryloyloxyethylamino)-7-nitro-2,1,3-benzoxadiazole (NBDAE) donor and rhodamine B-based potential acceptor (RhBHA) in the spirolactam form with pH and Hg^{2+}(Cu^{2+})-reactive characteristics were respectively copolymerized into the hydrophobic PS and thermoresponsive PNIPAM block of P(St-*co*-NBDAE)-*b*-P(NIPAM-*co*-RhBHA) amphiphilic diblock copolymers, where PS and PNIPAM represent polystyrene and poly(*N*-isopropylacrylamide). In aqueous solution, the FRET pair-labeled diblock copolymer self-assembles into nanosized micelles with NBDAE moieties located in the micellar cores and RhBHA in the thermoresponsive coronas. Because of that Hg^{2+} ions and acidic pH can induce the transformation of RhBHA from the nonfluorescent spirolactam form to highly fluorescent acyclic form, and the FRET process between NBDAE and RhBHA moieties, located respectively within micellar cores and coronas, can be effectively switched on. Thus, these nanosized micelles can serve as excellent ratiometric fluorescent probes for Hg^{2+} ions and pH, accompanied by fluorometric transition from green to orange and colorimetric change from almost colorless to pink. At a micellar concentration of 0.05 g/L and 25 °C, the detection limit of Hg^{2+} ions can be down to ~14.8 ppb. On the other hand, Cu^{2+} ions can quantitatively induce the ring-opening of RhBHA moieties and afford nonfluorescent residues, which can effectively quench the NBDAE emission. On the basis of the relative changes in NBDAE emission intensities, the Cu^{2+} detection limit can be down to ~4.3 ppb. Most importantly, the spatial distance of the FRET pair can be facilely tuned via thermo-induced collapse of PNIPAM micellar coronas, which dramatically increase the FRET efficiency and enhance the pH detection sensitivity. This work represents a proof-of-concept example of amphiphilic block copolymer micelles-based multifunctional ratiometric fluorescent probes for two types of metal ions (Hg^{2+} and Cu^{2+}), pH, and temperatures, which augurs well for their potential applications as nanocarriers with integrated functions such as imaging, sensing, and controlled-release of therapeutics.

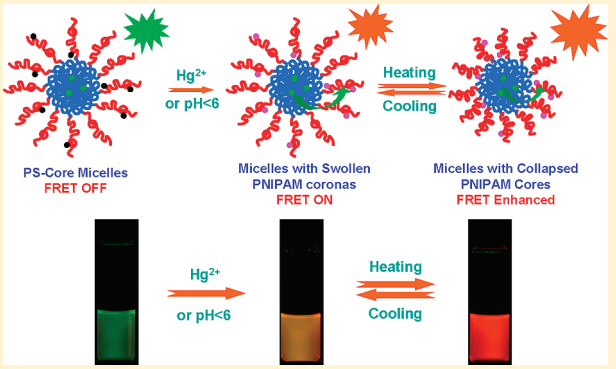

INTRODUCTION

As the third most frequently found and second most common toxic heavy metal in the list of the Agency for Toxic Substances and Disease Registry (ATSDR) of the U.S. Department of Health and Human Services, the mercury ion (Hg^{2+}) poses a huge threat to human beings and the environment due to its bioaccumulation, its ability to cause permanent damage, and its long residence in central nervous and endocrine systems.[1,2] Thus, it is quite imperative to screen suitable Hg^{2+} detection systems with high sensitivity and selectivity. Accordingly, numerous fluorometric and colorimetric Hg^{2+} probes have been developed based on small molecule chromophores,[3−33] conjugated polymers,[34−41] hybrid silica nanoparticles,[42−44] semiconductor quantum dots,[45,46] noble metal nanoparticles/nanoclusters,[47−52] biomolecules,[53−59] synthetic polymers,[60] and polymeric assemblies.[61−63] Current research focus in this area has concentrated on the development of Hg^{2+}-sensing systems with excellent aqueous solubility, improved selectivity and sensitivity, and high reliability and repeatability.[64] Most importantly, conventional Hg^{2+} probes have only been developed for single sensing functions. Considering their applications under complex circumstances such as in living cells and tissues, it would be quite advantageous to endow them with multiple sensing capabilities and other integrated functions such as the delivery of therapeutics.

Considering the reliability and repeatability of fluorometric sensing systems, probes based on analyte-induced changes in the

Received: January 17, 2011
Revised: April 12, 2011
Published: May 31, 2011

Scheme 1. Schematic Illustration for the Construction of P(St-*co*-NBDAE)-*b*-P(NIPAM-*co*-RhBHA) Amphiphilic Thermoresponsive Diblock Copolymer Micelles-Based Multifunctional Ratiometric Fluorescent Chemosensors for Metal Ions (Hg^{2+} and Cu^{2+}), pH, and Temperatures

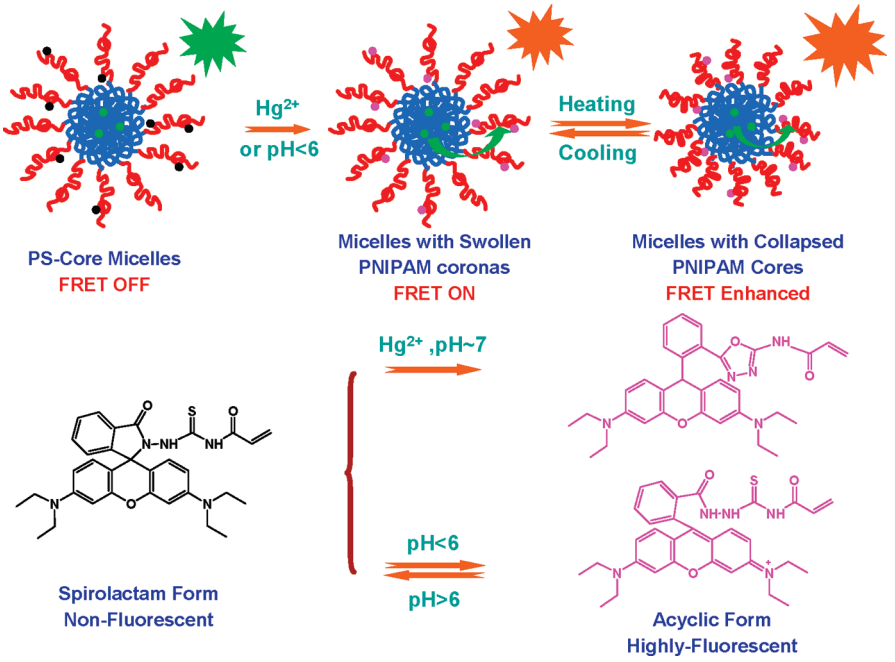

fluorescence intensity of single emission band possess inherent limits such as high background interference; thus, the fluctuation of detection conditions can seriously affect the accuracy of measurement. In this context, ratiometric fluorescent probes based on the fluorescence resonance energy transfer (FRET) principle or the introduction an internal reference dye have been designed, which allows for the simultaneous recording of emission intensities at two wavelengths and the "internal" self-calibration. The efficiency of FRET process is highly dependent on the relative distance ($R \sim 1-10$ nm) between donor and acceptor moieties, and is inversely proportional to R^6.[65,66] Thus, the successful construction of ratiometric fluorescent systems by involving the FRET principle relies on the accurate and optimized spatial distribution of FRET pairs. Moreover, if the spatial distribution of FRET dyes can be tuned by external stimuli or the presence of a specific analyte, then the integration of multiple sensing functions and the modulation of detection performance can be achieved.

In the past few years, several examples of small molecule-based ratiometric fluorescent Hg^{2+} probes have been reported. Some of them suffer from less satisfactory water solubility, and the sensing measurements need to be conducted in organic solvents or mixed aqueous/organic solution, as noted in a recent review article by Lippard et al.[64] This can seriously affect their practical in vivo sensing and imaging applications. Lippard et al.[67,68] recently reported two nice examples of purely aqueous-based ratiometric fluorometric Hg^{2+} sensors on the based of seminaphthofluorescein functionalized with aniline-derivatized pyridyl—amine—thioether chelating moieties. The seminaphthofluorescein fluorophore possesses two emission peaks at ~524 and 613 nm, and the intensity of the latter exhibits prominent increases upon addition of Hg^{2+} ions. Wu et al.[69] recently reported the construction of small molecule ratiometric fluorescent Hg^{2+} probes operated in aqueous media via the supramolecular binding between fluorescein-derivatized adamantine and β-cyclodextrin functionalized with Hg^{2+}-reactive rhodamine derivatives.

Considering their *in vivo* applications, small molecule fluorometric probes inherently possess limitations as they are subjected to rapid elimination and extravasation out of the vasculature, and this can considerably restrict the timing for measurements. Recently, synthetic polymers or polymeric assemblies covalently or physically attached with analyte-recognizing receptor or analyte-reactive moieties have been introduced to the design of novel sensing systems.[70,71] They can offer additional advantages such as improved water solubility, longer in vivo circulation times, and larger accumulation capacity due to the enhanced permeability and retention (EPR) effect. In addition, if the polymer matrix is responsive, multiple functions can be integrated by utilizing the reversible conformational changes, assembly/disassembly, and swelling/collapse of responsive polymer chains, polymeric assemblies, and microgels/nanogels, respectively.[72−82] Concerning responsive polymers or polymeric assemblies labeled with FRET pairs, it is also possible to more accurately control the spatial location and distribution of fluorescent dyes (such as within micellar cores and coronas) and tune the detection efficiencies.

Concerning polymeric assemblies-based Hg^{2+}-sensing systems, we recently reported the preparation of double hydrophilic block copolymers (DHBCs) bearing Hg^{2+}-reactive rhodamine B derivatives (RhBHA) in the thermoresponsive block, poly(ethylene oxide)-*b*-poly(*N*-isopropylacrylamide-*co*-RhBHA), PEO-*b*-P(NIPAM-*co*-RhBHA).[60] It can serve as multifunctional fluorometric sensors to pH, temperature, and Hg^{2+} ions. In addition, the detection sensitivity to Hg^{2+} ions and pH could be dramatically tuned at elevated temperatures due to thermo-induced formation of micelles possessing hydrophobic cores. In this case, Hg^{2+} and acidic pH can induce the chemical transformation of RhBHA moieties from nonfluorescent spirolactam form to the highly fluorescent acyclic form. It is worthy of

Scheme 2. Synthesis of Well-Defined Amphiphilic Thermoresponsive Diblock Copolymers, P(St-*co*-NBDAE)-*b*-P(NIPAM-*co*-RhBHA), via Sequential RAFT Polymerizations

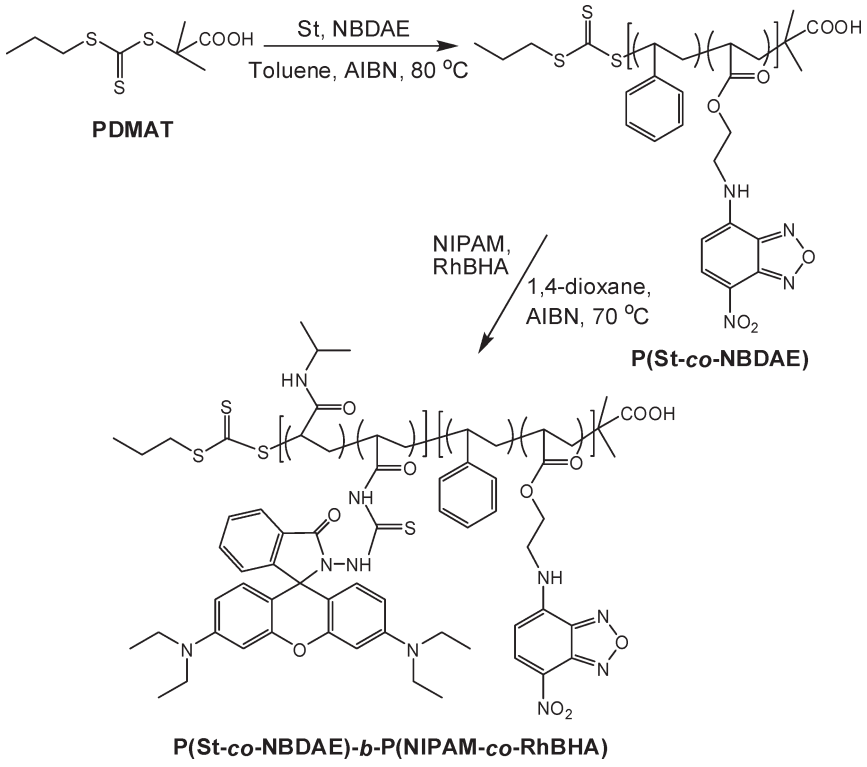

noting that this responsive polymeric assemblies-based Hg^{2+}-sensing system relies on changes in fluorescence intensities of a single emission band, i.e., nonratiometric sensing. Moreover, micelles of PEO-*b*-P(NIPAM-*co*-RhBHA) DHBCs only form at elevated temperatures and will dissociate into unimers upon cooling to room temperature. On the other hand, it has been well-established that amphiphilic block copolymer micelles are much more structurally stable. Thus, it is highly desirable to construct amphiphilic block copolymer micelles-based sensing systems with multifunctional ratiometric fluorescent sensing capabilities. Just recently, we reported on the construction of amphiphilic thermoresponsive block copolymer micelles containing one type of FRET donor and two types of potential FRET acceptors, and emission of the latter two can be off/on switched by pH variation and UV irradiation.[83] This novel type of micelles exhibit multicolor emission modulated by temperature, pH, and UV irradiation. On the basis of the two previously reported works, we feel that it is quite advantageous to further develop amphiphilic block copolymer micelles-based ratiometric fluorescent Hg^{2+} ion-sensing systems integrated with other probing functions (such as pH and temperatures).

In this work, we report on the fabrication of amphiphilic thermoresponsive diblock copolymer micelles-based multifunctional ratiometric fluorescent chemosensors for metal ions (Hg^{2+} and Cu^{2+}), pH, and temperatures (Scheme 1). FRET pair consisting of 4-(2-acryloyloxyethylamino)-7-nitro-2,1,3-benzoxadiazole (NBDAE) donor and rhodamine B-based potential acceptor (RhBHA) in the spirolactam form with pH and Hg^{2+}- (Cu^{2+}-) reactive characteristics were respectively copolymerized into the hydrophobic poly(styrene) (PS) and thermoresponsive PNIPAM block of P(St-*co*-NBDAE)-*b*-P(NIPAM-*co*-RhBHA) amphiphilic diblock copolymers (Schemes 1 and 2). We investigated in detail the Hg^{2+}- and Cu^{2+}-sensing capabilities of amphiphilic block copolymer micelles bearing NBDAE and RhBHA moieties respectively within the micellar cores and coronas. The ratiometric fluorometric pH and thermal sensing of diblock copolymer micelles and the effects of thermo-induced collapse of responsive micellar coronas on the pH detection sensitivity were also examined. To the best of our knowledge, this work represents a proof-of-concept example of amphiphilic block copolymer micelles-based multifunctional ratiometric fluorescent probes for two types of metal ions (Hg^{2+} and Cu^{2+}), pH, and temperatures, which augurs well for their potential applications as nanocarriers with integrated functions such as imaging, sensing, and controlled-release nanocarriers of therapeutics.

EXPERIMENTAL SECTION

Materials. *N*-Isopropylacrylamide (NIPAM, 97%, Tokyo Kasei Kagyo Co.) was recrystallized twice from a mixture of *n*-hexane and benzene (v/v = 2:1) prior to use. Styrene (St, 99.5%, Beijing Chemical Factory) was successively washed with aqueous NaOH (5.0 wt %) and saturated NaCl solution, and then distilled over CaH_2 at reduced pressure. 4-Chloro-7- nitrobenzofurazan (NBD−Cl, 99%, Alfa), rhodamine B (RhB, Acros) were used as received. Aminoethanol and acryloyl chloride (Sinopharm Chemical Reagent Co.) were distilled prior to use. 2,2′-Azoisobutyronitrile (AIBN) was recrystallized from 95% ethanol. Potassium thiocyanate (KSCN) and hydrazine hydrate (Sinopharm Chemical Reagent Co.) were used as received. Tetrahydrofuran (THF), toluene, methanol, 1,4-dioxane, and all the other solvents were used as received. Nitrate salts (K^+, Na^+, Li^+, Co^{2+}, Cd^{2+}, Pb^{2+}, Zn^{2+}, Fe^{2+}, Fe^{3+}, Ca^{2+}, Ag^+, Cu^{2+}, and Hg^{2+}) were used for all sensing experiments. Water was deionized with a Milli-Q SP reagent water system (Millipore) to a specific resistivity of 18.2 MΩcm.

dx.doi.org/10.1021/ma2001146 |*Macromolecules* 2011, 44, 4699–4710

4-(2-Acryloyloxyethylamino)-7-nitro-2,1,3-benzoxa-diazole (NBDAE),[73,84] RhBHA,[60] and *S*-1-propyl-*S*′-(α,α′-dimethyl-α′′-acetic acid)trithiocarbonate (PDMAT)[85] were synthesized according to previously reported literature procedures.

Sample Synthesis. Typical synthetic approaches employed for the preparation of P(St-*co*-NBDAE)-*b*-P(NIPAM-*co*-RhBHA) amphiphilic diblock copolymers are shown in Scheme 2. The structural parameters of P(St-*co*-NBDAE) precursor and the diblock copolymer are shown in Table S1 (Supporting Information).

Synthesis of P(St-co-NBDAE) (Scheme 2). Typical RAFT polymerization procedures employed for the synthesis of NBDAE-labeled P(St-*co*-NBDAE)$_{20}$ precursor are as follows. St (5.21 g, 50 mmol), NBDAE (27.8 mg, 0.1 mmol), PDMAT (0.119 g, 0.5 mmol), AIBN (8.2 mg, 0.05 mmol), and 1,4-dioxane (5.21 g) were charged into a reaction tube equipped with a magnetic stirring bar. The tube was carefully degassed by three freeze−pump−thaw cycles and then sealed under vacuum. After thermostatting at 80 °C in an oil bath and stirring for 12 h, the reaction tube was quenched into liquid nitrogen, opened, and diluted with THF; the mixture was then precipitated into an excess of methanol. The above dissolution−precipitation cycle was repeated for three times. After drying in a vacuum oven overnight at 25 °C, P(St-*co*-NBDAE)$_{20}$ was obtained as a yellowish powder (1.06 g, yield: 20%, M_n = 2.2 kDa, M_w/M_n = 1.08, Figures S1 and S2).

Synthesis of P(St-co-NBDAE)-b-P(NIPAM-co-RhBHA) Amphiphilic Diblock Copolymer (Scheme 2). Typical procedures employed for the synthesis of amphiphilic diblock copolymer are as follows. P(St-*co*-NBDAE)$_{20}$ (0.232 g, 0.1 mmol), NIPAM (1.13 g, 10 mmol), RhBHA (28.5 mg, 0.05 mmol), AIBN (2 mg, 12 μmol), and 1,4-dioxane (2.0 g) were charged into a reaction tube equipped with a magnetic stirring bar. The tube was carefully degassed by three freeze−pump−thaw cycles and then sealed under vacuum. After thermostatting at 70 °C in an oil bath and stirring for 2 h, the reaction tube was quenched into liquid nitrogen, opened, and diluted with THF; the mixture was then precipitated into an excess of diethyl ether. The above dissolution−precipitation cycle was repeated for three times. The obtained diblock copolymer was further treated with excess AIBN (20 equiv) in THF. After reaction at 70 °C for 2 h, the amphiphilic diblock copolymer was precipitated into excess diethyl ether three times and dried in vacuum at 25 °C overnight. P(St-*co*-NBDAE)$_{20}$-*b*-P(NIPAM-*co*-RhBHA)$_{54}$ was obtained as a slightly pink powder (0.72 g, yield: 52%, M_n = 8.6 kDa, M_w/M_n = 1.12, Figures S1 and S2). The molar content of NBDAE moieties (relative to the PS block) and RhBHA moieties (relative to the PNIAPM block) were determined to be ∼0.2 and ∼0.5 mol %, respectively, based on standard UV absorbance calibration curves. According to similar procedures, additional amphiphilic diblock copolymers with varying block lengths, P(St-*co*-NBDAE)$_{20}$-*b*-P(NIPAM-*co*-RhBHA)$_{106}$ and P(St-*co*-NBDAE)$_{41}$-*b*-P(NIPAM-*co*-RhBHA)$_{56}$, and control samples, PS$_{20}$-*b*-P(NIPAM-*co*-RhBHA)$_{56}$, PS$_{20}$-*b*-P(DMA-*co*-RhBHA)$_{57}$, and P(St-*co*-NBDAE)$_{20}$-*b*-PNIPAM$_{56}$ were also synthesized. Relevant structural parameters are summarized in Table S1 (Supporting Information).

Preparation of Micellar solutions. Typical procedures employed for the preparation of micellar solutions are as follows. 1.0 mg of P(St-*co*-NBDAE)-*b*-P(NIPAM-*co*-RhBAM) amphiphilic diblock copolymer was dissolved in 1 mL of DMF. Under vigorous stirring, 9 mL of deionized water was then slowly added. After the addition process is completed, the micellar solution was further stirred for another 4 h. DMF was then removed by dialysis (MW cutoff, 3500 Da) against deionized water for 12 h. During this process, fresh deionized water was replaced approximately every 6 h.

Cell Culture and in Vitro Fluorescent Imaging of Hg^{2+} Ions. HeLa cells were cultured in Dulbecco's modified Eagle medium (DMEM) supplemented with 10% fetal bovine serum (FBS), penicillin (100 units/mL), and streptomycin (100 μg/mL) at 37 °C in a CO_2/air (5:95) incubator for 2 days. For fluorescence imaging, cells were transferred to DMEM containing 1% FBS and 0.1 g/L P(St-*co*-NBDAE)$_{20}$-*b*-P(NIPAM-*co*-RhBHA)$_{54}$ micellar solution at 37 °C in a CO_2/air (5:95) incubator for 4 h. The cells were washed twice with PBS buffer prior to the addition of Hg^{2+} ions. Hg^{2+} ions (5.0 equiv. relative to RhBHA moieties) were then introduced to the cultured cells, and the mixture was further incubated for 30 min.

Characterization. All ^{1}H nuclear magnetic resonance (NMR) spectra were recorded on a Bruker AV300 NMR spectrometer (resonance frequency of 300 MHz for ^{1}H) operated in the Fourier transform mode. $CDCl_3$ was used as the solvent. Molecular weights and molecular weight distributions were determined by gel permeation chromatography (GPC) equipped with Waters 1515 pump and Waters 2414 differential refractive index detector (set at 30 °C). The detection components used a series of two linear Styragel columns (HR2 and HR4) at an oven temperature of 45 °C. The eluent was THF at a flow rate of 1.0 mL/min. A series of low polydispersity polystyrene standards were employed for calibration. Dynamic and static laser light scattering (LLS) measurements were conducted on a commercial spectrometer (ALV/DLS/SLS-5022F) equipped with a multitau digital time correlator (ALV5000) and a cylindrical 22 mW UNIPHASE He−Ne laser (λ_0 = 632 nm) as the light source. Scattered light was collected at a fixed angle of 90° for duration of ∼5 min. Distribution averages and particle size distributions were computed using cumulants analysis and CONTIN routines. Equilibrium surface tensions were measured using a JK99B tensiometer with a platinum plate. The measuring accuracy of the device as reported by the manufacturer is ±0.1 mN/m. The reported surface tension was the average of five measurements that were taken after allowing each of the solutions to equilibrate in the instrument fixed at 25.0 °C. Fluorescence spectra were recorded using a F-4600 (Hitachi) spectrofluorometer. The temperature of the water-jacketed cell holder was controlled by a programmable circulation bath. The slit widths were both set at 5 nm for excitation and emission. Unless specified, all fluorescence spectra were recorded after incubation for 10 min upon the addition of each batch of aqueous solution of metal ions. All UV−vis spectra were acquired on a RF-5301/PC (Shimadzu) spectrofluorometer. A thermostatically controlled couvette was employed and the heating rate was 0.2 °C min^{-1}. Differential scanning calorimetry (DSC) measurements were conducted on a DSC TA-60WS thermal analysis system (Shimadzu, Japan). Samples were first heated from 0 to 200 °C at a heating rate of 10 °C/min under nitrogen atmosphere, followed by cooling to 20 °C at a rate of 10 °C/min after stopping at 200 °C for 3 min, and finally heating to 200 °C at a rate of 10 °C/min. Glass transition temperature (T_g) was determined as the midpoint of the transition of the final heating process. Fluorescence images of HeLa cells before and after addition of Hg^{2+} ions were acquired using Nikon Eclipse TE2000-U inverted microscopy at 37 °C.

RESULTS AND DISCUSSION

Synthesis of P(St-*co*-NBDAE)-*b*-P(NIPAM-*co*-RhBHA). Well-defined amphiphilic diblock copolymer with the hydrophobic PS block and thermoresponsive PNIPAM block respectively labeled with NBDAE as the FRET donor and rhodamine B-based potential FRET acceptor (RhBHA) were synthesized via sequential RAFT polymerizations (Scheme 2). The RAFT copolymerization of styrene with NBDAE facilely afforded narrow-disperse P(St-*co*-NBDAE) precursor (Figure S2 (Supporting Information)). NBDAE content in the P(St-*co*-NBDAE) block was determined to be ∼0.2 mol %. The subsequent RAFT copolymerization of NIPAM and RhBHA was then conducted by utilizing P(St-*co*-NBDAE) as the macroRAFT agent, affording the amphiphilic thermoresponsive diblock copolymer with RhBHA

content in the P(NIPAM-*co*-RhBHA) block being ~0.5 mol %. GPC analysis revealed that the amphiphilic diblock copolymer possesses a relatively narrow polydispersity (M_n = 8.6 kDa, M_w/M_n = 1.12). The degrees of polymerization (DPs) of PS and PNIPAM blocks were determined to be 20 and 54, respectively by ^{1}H NMR analysis (Figure S1 (Supporting Information)). Thus, the diblock copolymer was denoted as P(St-*co*-NBDAE)$_{20}$-*b*-P(NIPAM-*co*-RhBHA)$_{54}$. The structural parameters of P(St-*co*-NBDAE)$_{20}$ precursor and P(St-*co*-NBDAE)$_{20}$-*b*-P(NIPAM-*co*-RhBHA)$_{54}$ diblock copolymer are summarized in Table S1 (Supporting Information). According to similar procedures, additional amphiphilic diblock copolymers with varying block lengths and other control samples were also synthesized and their structural parameters are summarized in Table S1 (Supporting Information).

In aqueous solution, the amphiphilic diblock copolymer can self-assemble into micelles consisting of hydrophobic P(St-*co*-NBDAE) cores and thermoresponsive P(NIPAM-*co*-RhBHA) coronas (Scheme 1). Surface tensiometry measurements revealed that diblock copolymer micelles possess a critical micellization concentration (CMC) of ~3.0 mg/L (Figure S3 (Supporting Information)). Such a low CMC can be ascribed to the highly hydrophobic nature of PS block. As shown in Figure S4 (Supporting Information), temperature-dependent optical transmittance measurements of the micellar solution of P(St-*co*-NBDAE)$_{20}$-*b*-P(NIPAM-*co*-RhBHA)$_{54}$ at a concentration of 0.5 g/L revealed that the micelles tend to aggregate above the critical thermal phase transition temperature of ~28 °C, which is due to the lower critical solution temperature (LCST) phase transition behavior of PNIPAM coronas. As compared to the LCST of PNIPAM homopolymers (~32 °C), the decreased LCST of P(St-*co*-NBDAE)$_{20}$- *b*-P(NIPAM-*co*-RhBHA)$_{54}$ should be ascribed to two cooperative factors. First, PNIPAM chains were grafted at the surface of hydrophobic PS core. Second, PNIPAM chains within the micellar corona are densely packed relative to that of free PNIPAM chains and this will decrease the LCST according to previous reports concerning the thermal phase transition of PNIPAM star polymers and PNIPAM brushes grafted at the surface of inorganic nanoparticles.[86−88]

As expected, at a much lower concentration (0.05 g/L), we can observe the thermo- induced collapse of PNIPAM coronas, as revealed by dynamic LLS measurements (Figure S5 (Supporting Information)). At 25 °C, P(St-*co*-NBDAE)$_{20}$-*b*-P(NIPAM-*co*-RhBHA)$_{54}$ micelles possess an intensity-average hydrodynamic diameter, $\langle D_h \rangle$, of ~71 nm and a size polydispersity, μ_2/Γ^2 of 0.061. Static LLS measurements revealed an $M_{w,app} = 5.88 \times 10^6$ and an average aggregation number per micelles, N_{agg}, of 610 (Figure S6 (Supporting Information)). Thus, there exist ~24.3 NBDAE and ~164.7 RhBHA moieties within each micelle. Upon heating to 40 °C, which is above the LCST of PNIPAM coronas, the micelles possess an $\langle D_h \rangle$, of ~40 nm and a polydispersity of 0.056 (Figure S5 (Supporting Information)). This clearly suggested the thermo-induced collapse of PNIPAM coronas. Moreover, as the FRET donors (NBDAE) and pH/Hg^{2+}-reactive FRET acceptors are randomly distributed within micellar cores and coronas, respectively, the thermo-induced collapse of micellar coronas can considerably lead to closer proximity between FRET donor and acceptor dyes and enhanced FRET efficiencies.

P(St-*co*-NBDAE)-*b*-P(NIPAM-*co*-RhBHA) Micelles as Multifunctional Sensors for Metal Ions, pH, and Temperatures. Compared to conventional fluorometric sensors based on changes in the fluorescence intensity of a single emission band, sensing systems by employing the FRET principle can effectively eliminate background interference and the fluctuation of detection conditions via the self-calibration of two emission bands at different wavelengths. In this work, we employed green-emitting NBDAE chromophore as the FRET donor and initially nonfluorescent RhBHA moiety in the spirolactam form as the potential FRET acceptor. It has been previously reported that the presence of Hg^{2+} ions or acidic pH can induce the transformation of RhBHA from the nonfluorescent spirolactam form to the highly fluorescent acyclic form,[60] and this can effectively switch on the FRET process between NBDAE and acyclic RhBHA moieties respectively located within micellar cores and coronas (Scheme 1).

NBDAE moieties possess a fluorescence emission band with a maximum at ~518 nm (Figure S7 (Supporting Information)). Though RhBHA moieties in the spirolactam form exhibit no obvious absorbance in the range of 450−650 nm, RhBHA moieties in the acyclic form exhibit a broad absorbance peak with a maximum at ~565 nm. As shown in Figure S7 (Supporting Information), the emission spectrum of NBDAE overlaps quite well with the absorbance spectrum of acyclic RhBHA, indicating that effective FRET process can occur between NBDAE and acyclic RhBHA in the presence of Hg^{2+} ions or upon lowering solution pH. When the aqueous solution of micellar assemblies was excited at 470 nm, the excited NBDAE moieties could transfer energy to the acyclic RhBHA moieties in the ground state. Previously, Wu et al.[89] reported the construction of PEO-*b*-PS micelle-based ratiometric fluorometric Fe^{3+}-sensing system. In that case, the FRET donor was physically embedded within micellar cores and the FRET acceptor was presumably at the core−shell interface. The progressive diffusion of physically embedded dyes out of the micelles might lead to the worsening of accuracy and repeatability of sensing experiments. In addition, it is quite difficult to accurately locate and control the spatial distribution of FRET pair within the micellar assemblies. In the current study, both FRET donor and acceptor dyes were covalently attached to the amphiphilic diblock copolymers, and this rational design can endow it with long-term structural integrity and stable sensing performance. Moreover, NBDAE and RhBHA dyes are randomly located within micellar cores and coronas, and the spatial proximity between the FRET pair can be tuned via thermo-induced collapse of thermoresponsive coronas (Scheme 1).

To investigate the metal ion-sensing capability of amphiphilic diblock copolymer micelles-based system, a series of fluorescence measurements upon addition of Hg^{2+} ions were conducted. At first, we attempted to determine the time period required for the reaction-induced changes in fluorescent intensity to reach the final equilibrium. Tae et al.[3,10] previously reported small molecule Hg^{2+} probes based on leuco-rhodamine derivative, and the presence of Hg^{2+} ions resulted in desulfurization reaction to turn on the fluorescence emission. They also reported the sensing kinetics and found that the reaction is accomplished within ~1 min and $t_{1/2}$ was determined to be ~0.2 s at room temperature. This feature offers the possibility of in vivo real-time monitoring of Hg^{2+} ions. In the current system, the initially nonfluorescent RhBHA moieties were located within coronas of P(St-*co*-NBDAE)$_{20}$-*b*-P(NIPAM-*co*-RhBHA)$_{54}$ micelles and this might lead to different reaction kinetics. Upon addition of varying amounts of Hg^{2+} ions (0.1, 0.5, 1.0, and 5.0 equiv), the reaction kinetics was then monitored by recording the time-dependent

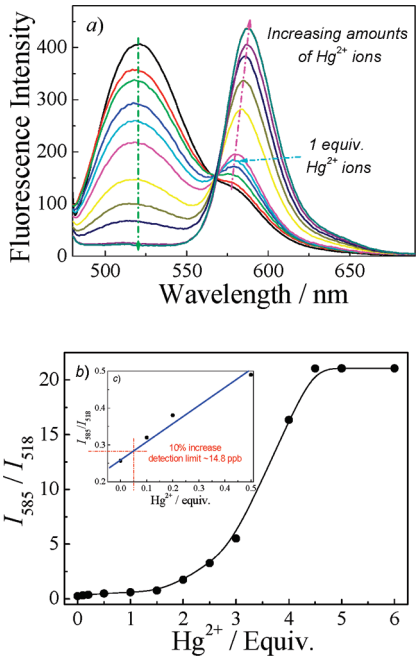

Figure 1. (a) Fluorescence emission spectra and (b) fluorescence intensity ratio changes of 0.05 g/L micellar solutions of P(St-*co*-NBDAE)$_{20}$-*b*-P(NIPAM-*co*-RhBHA)$_{54}$ at pH 7 upon addition of 0−6.0 equiv. Hg^{2+} ions at 25 °C ([RhBHA] = 1.57 μM, λ_{ex} = 470 nm, slit width: Ex. 5 nm, Em. 5 nm). The inset (c) shows the fluorescence intensity ratio changes upon addition of 0−0.5 equiv. Hg^{2+} ions (relative to the RhBHA moieties) and the determination of detection limit.

changes of fluorescence intensities (Figure S8 (Supporting Information)). It was found that in all cases, the reaction is completed within ~5 min. Upon addition of 5.0 equiv. Hg^{2+} ions into 0.05 g/L micellar solution of P(St-*co*-NBDAE)$_{20}$-*b*-P(NIPAM-*co*-RhBHA)$_{54}$, $t_{1/2}$ was determined to be ~1.5 min. Moreover, the final stabilized fluorescence intensities increase with increasing Hg^{2+} concentrations. Thus, in subsequent sections all fluorescence spectra were recorded after incubation for 10 min, unless specified, upon the addition of each batch of aqueous solution of metal ions to make sure that the reaction induced by the previous addition was finished.

First, we examined the Hg^{2+}-sensing capability of the micellar solution of P(St-*co*-NBDAE)$_{20}$-*b*-P(NIPAM-*co*-RhBHA)$_{54}$ diblock copolymers at 25 °C. Typical fluorescence spectra recorded for the micellar solution (0.05 g/L, [NBDAE] = 0.23 μM, [RhBHA] = 1.57 μM) upon addition of Hg^{2+} ions are shown in Figure 1. In the absence of Hg^{2+} ions, we can apparently observe two well-resolved emission peaks centered at ~518 and 580 nm, respectively. The one at 518 nm can be safely ascribed to NBDAE emissions as compared to the emission spectrum of P(St-*co*-NBDAE)$_{20}$ recorded in THF (Figure S6 (Supporting Information)). The emission band at ~580 nm is quite weak, which should be ascribed to RhBHA moieties existing in the ring-opened acyclic form. Preliminary experiments revealed that the presence of trace amount of fluorescent RhBHA in the acyclic form might result from the RAFT polymerization and subsequent purification and storage processes. Upon addition of Hg^{2+} ions, we can clearly observe the decrease of NBDAE emission band at ~518 nm and the prominent increase of RhBHA emission intensity, clearly suggesting that the FRET process between NBDAE and RhBHA moieties has been effectively switched on. With increasing amount of Hg^{2+} ions, we can also discern a slight red-shift from ~580 to 585 nm for the RhBHA emission maximum (Figure 1). As shown in Figure 1b, fluorescence emission intensity ratios (I_{585}/I_{518}) dramatically increased upon addition of Hg^{2+} ions and stabilized out in the presence of >5.0 equiv of Hg^{2+} ions (relative to RhBHA residues). Accompanied with the increase of fluorescence intensity ratios, the absorbance intensity at ~565 nm characteristic of acyclic RhBHA also exhibit considerable increase upon addition of Hg^{2+} ions (Figure S9 (Supporting Information)). The diagnostic absorbance peak of NBDAE moieties, which should locate at ~470 nm, is barely visible, which might be ascribed to the facts that the NBDAE content is relatively low (0.23 μM) and that they are selectively embedded within the micellar cores.[83]

A closer examination of Figure 1b and Figure S9 (Supporting Information)revealed that the I_{585}/I_{518} emission intensity ratio almost levels off at >5.0 equiv. Hg^{2+} ions and the absorbance of acyclic RhBHA also tends to stabilize out at >5.0 equiv. Hg^{2+} ions. However, the latter almost linearly increase with the Hg^{2+} concentration (0−5 equiv), whereas for the former, the emission intensity ratio exhibits a slow increase in the range of 0−2.0 equiv of Hg^{2+} concentration and the subsequent abrupt increase. We have ascribed this apparent discrepancy to the fact that the former reflects the changes of intensity ratios between acyclic RhBHA and NBDAE emissions, whereas for the latter, only the absorbance of acyclic RhBHA was measured. We further measured the emission of acyclic RhBHA moieties only when excited at 560 nm (which can not excite NBDAE moieties), and the results are shown in Figure S10 (Supporting Information). We can indeed observe that the emission of acyclic RhBHA when excited at 560 nm exhibits comparable changes to the absorbance (as shown in Figure S9 (Supporting Information)) upon addition of 0−6.0 equiv of Hg^{2+} ions.

If we define the detection limit as the Hg^{2+} concentration at which a 10% increase in fluorescence intensity ratios (I_{585}/I_{518}) can be measured by employing 0.05 g/L micellar solution, the Hg^{2+} ions detection limit can be determined to be ~14.8 ppb (Figure 1c). Theoretically, the detection limit and sensitivity in specific concentration ranges can be further improved by optimizing dye labeling contents and relative block lengths, and by adjusting micellar concentrations. To confirm these issues, we further synthesized two amphiphilic diblock copolymers with varying block lengths, P(St-*co*-NBDAE)$_{20}$-*b*-P(NIPAM-*co*-RhBHA)$_{106}$ and P(St-*co*-NBD)$_{41}$-*b*-P(NIPAM-*co*-RhBHA)$_{56}$ (see Table S1 (Supporting Information)) with dye molar contents in both blocks comparable to those of P(St-*co*-NBDAE)$_{20}$-*b*-P(NIPAM-*co*-RhBHA)$_{54}$. It was found from Figure S11 (Supporting Information) that for the three diblock copolymers, the Hg^{2+} detection limit does not vary considerably. However, due to the changes of FRET donor/acceptor molar ratios and block lengths, the Hg^{2+} detection sensitivity in the specific medium concentration range (0.5−2.0 ppm) can be prominently modulated.[90] Compared to that of P(St-*co*-NBDAE)$_{20}$-*b*-P(NIPAM-*co*-RhBHA)$_{54}$, the CMC of P(St-*co*-NBDAE)$_{41}$-*b*-P(NIPAM-*co*-RhBHA)$_{56}$ decreased to ~0.8 mg/L. We then tried to further improve the detection limit by decreasing the concentration of micellar solution of P(St-*co*-NBDAE)$_{41}$-*b*-P(NIPAM-*co*-RhBHA)$_{56}$. It was found that at a micellar concentration of 0.01 g/L, the Hg^{2+} detection limit can be down to ~4.3 ppb. Another notable feature of P(St-*co*-NBDAE)-*b*-P(NIPAM-*co*-RhBHA) micelles-based ratiometric fluorescent

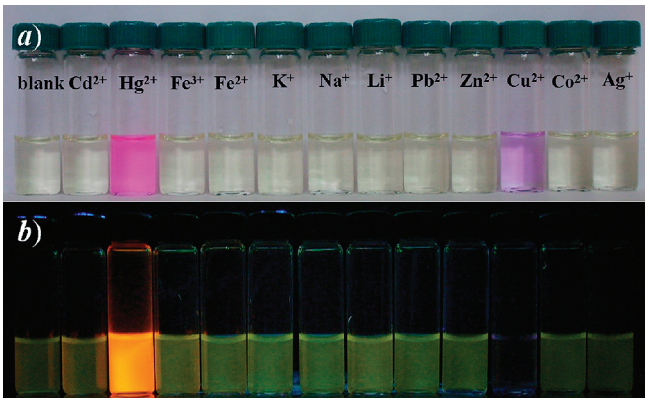

Figure 2. Optical photographs recorded under (a) visible light and (b) UV light (365 nm) for 0.1 g/L micellar solutions (pH 7, 25 °C) of P(St-*co*-NBDAE)$_{20}$-*b*-P(NIPAM-*co*-RhBHA)$_{54}$ at ~10 min after the addition of 5.0 equiv of Cd^{2+}, Hg^{2+}, Fe^{3+}, Fe^{2+}, K^+, Na^+, Li^+, Pb^{2+}, Zn^{2+}, Cu^{2+}, Co^{2+}, and Ag^+ ions, respectively.

sensing system is that the aggregate sizes can be tuned by relative block lengths, which is quite advantageous to modulate their retention time within cells and tissues considering their potential applications for in vivo sensing and imaging purposes.

In the next step, the detection selectivity toward Hg^{2+} ions for the micellar solution of P(St-*co*-NBDAE)$_{20}$-*b*-P(NIPAM-*co*-RhBHA)$_{54}$ was examined (Figures 2−4). Among a series of cations including K^+, Na^+, Li^+, Co^{2+}, Cd^{2+}, Pb^{2+}, Zn^{2+}, Fe^{2+}, Fe^{3+}, Ca^{2+}, Ag^+, Cu^{2+}, and Hg^{2+} ions (5 equiv), it was found that only Hg^{2+} ions can induce the apparent fluorometric transition from green to orange at ~10 min after the addition of metal ions, which can be clearly discerned by the naked eye (Figure 2). Note that from Figure 2, we can also observe the Hg^{2+}-induced colorimetric transition from almost colorless to pink. Upon addition of Cu^{2+} ions, a colorimetric transition from almost colorless to purple can be discerned under visible light, which is similar to those reported for PEO$_{113}$-*b*-P(NIPAM-*co*-RhBHA)$_{69}$ system.[60] Under UV 365 nm irradiation, the initially green fluorescence emission of micellar solution was almost turned off upon the addition of Cu^{2+} ions. Note that in the previous work,[60] PEO$_{113}$-*b*-P(NIPAM-*co*-RhBHA)$_{69}$ solutions are always nonfluorescent before and after the addition of Cu^{2+} ions.

Fluorescence and absorption measurements were further conducted in the presence of various metal ions (5 equiv. relative to the RhBHA moieties). The fluorescence measurements (Figure 3) revealed that only Hg^{2+} ions induce the most prominent changes of fluorescence intensity ratios. Ag^+ ions also induce the ring-opening reaction of RhBHA moieties to some extent and lead to the decrease and increase of NBDAE and acyclic RhBHA emission bands, respectively (Figure 3a), but only after a relatively long incubation period (~5 h) after the addition. This might be ascribed to the relatively high affinity between Ag^+ ions and thiourea moieties.[91] Though Cu^{2+} ions also induced the colorimetric transition from almost colorless to purple (Figure 2), the fluorescence emission intensity are quite weak at wavelengths spanning across the emission bands of NBDAE and acyclic RhBHA (Figure 3). Thus, for the current polymeric micelles-based sensing system, it is facile to discriminate Hg^{2+} ions from Cu^{2+} ions based on their drastically different fluorometric responses. On the other hand, the discrimination of Ag^+ ions can also be achieved

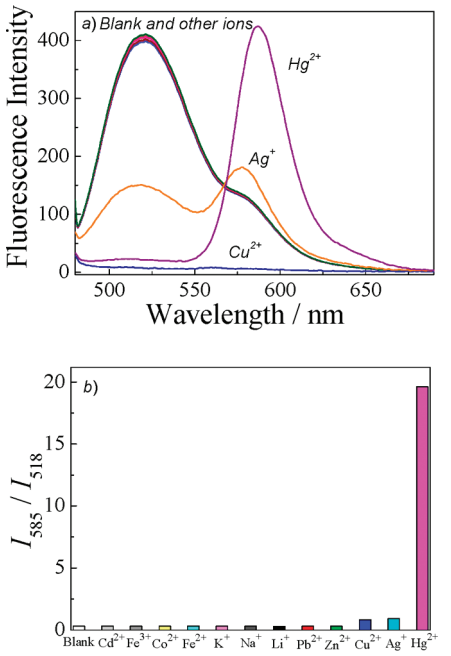

Figure 3. (a) Fluorescence emission spectra and (b) fluorescence intensity ratio changes of micellar solution (0.05 g/L) of P(St-*co*-NBDAE)$_{20}$-*b*-P(NIPAM-*co*-RhBHA)$_{54}$ at pH 7 in the presence of 5.0 equiv of Cd^{2+}, Fe^{3+}, Co^{2+}, Fe^{2+}, K^+, Na^+, Li^+, Pb^{2+}, Zn^{2+}, Cu^{2+} Ag^+, and Hg^{2+} ions, respectively ([RhBHA] = 1.57 μM; λ_{ex} = 470 nm; slit width, Ex. 5 nm, Em. 5 nm). All spectra were recorded 5 h after the addition of various metal ions.

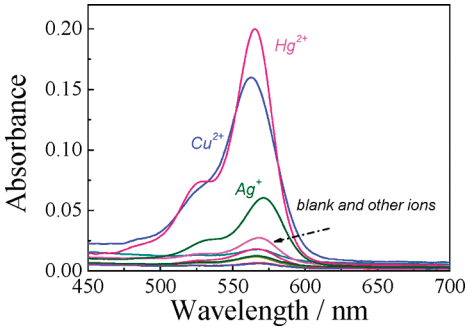

Figure 4. UV−vis absorption spectra recorded for 0.05 g/L micellar solution of P(St-*co*-NBDAE)$_{20}$-*b*-P(NIPAM-*co*-RhBHA)$_{54}$ at pH 7 upon addition of 5 equiv of Cd^{2+}, Fe^{3+}, Co^{2+}, Fe^{2+}, K^+, Na^+, Li^+, Pb^{2+}, Zn^{2+}, Cu^{2+} Ag^+, and Hg^{2+} ions, respectively. All spectra were recorded 5 h after the addition of various metal ions.

based on the quite extended incubation time (~5 h) need for the colorimetric and fluorometric transitions, as compared to the relatively fast response time (<10 min) of Hg^{2+} and Cu^{2+} ions (Figure 2).

UV−vis absorption measurements were further conducted to probe the underlying mechanism for colorimetric and fluorometric transitions occurred upon addition of different types of metal ions (Figure 4). The absorption spectra revealed that acyclic RhBHA moieties resulting from the ring-opening reaction induced by Hg^{2+} and Cu^{2+} ions exhibit strong absorbance at 565 and 563 nm, respectively, whereas that induced by Ag^+ ions exhibits much weaker absorbance compared to those of Hg^{2+} and Cu^{2+} ions. We propose that both Hg^{2+} and Cu^{2+} ions can

dx.doi.org/10.1021/ma2001146 |*Macromolecules* 2011, 44, 4699–4710

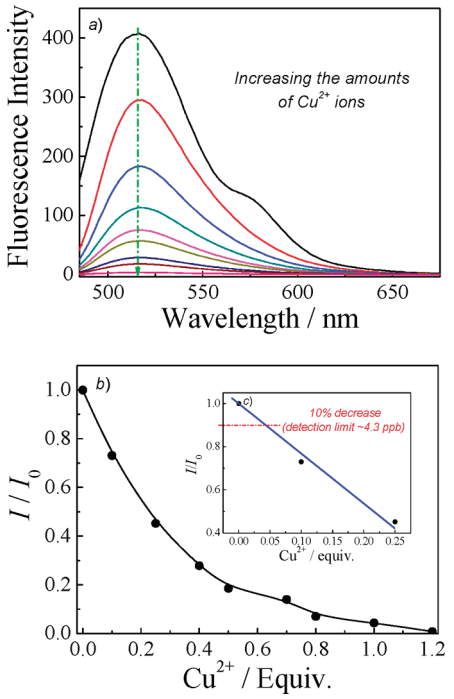

Figure 5. (a) Fluorescence emission spectra and (b) fluorescence intensity changes of 0.05 g/L micellar solution of P(St-*co*-NBDAE)$_{20}$-*b*-P(NIPAM-*co*-RhBHA)$_{54}$ at pH 7 upon addition of Cu^{2+} ions (0−1.2 equiv) at 25 °C ([RhBHA] = 1.57 μM; λ_{ex} = 470 nm; slit width, Ex. 5 nm, Em. 5 nm). The inset (c) shows the fluorescence intensity changes upon addition of 0−0.25 equiv. Cu^{2+} ions (relative to the RhBHA moieties) and the determination of detection limit.

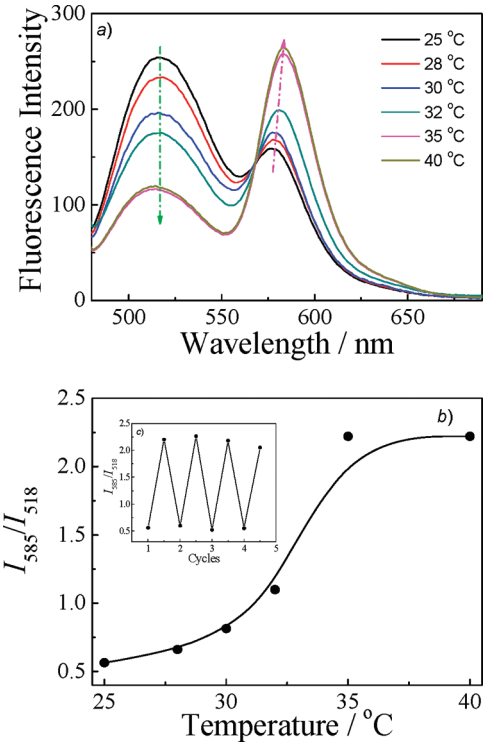

Figure 6. (a) Fluorescence emission spectra, (b) fluorescence intensity ratio changes of 0.05 g/L micellar solution of P(St-*co*-NBDAE)$_{20}$-*b*-P(NIPAM-*co*-RhBHA)$_{54}$ in the presence 1 equiv. Hg^{2+} ions (relative to RhBHA moieties) in the temperature range of 25−40 °C. The inset (c) shows fluorescence intensity ratio changes of the micellar solution ([RhBHA] = 1.57 μM; λ_{ex} = 470 nm; slit width, Ex. 5 nm, Em. 5 nm) upon repeated heating (40 °C) and cooling (25 °C) cycles.

induce the ring-opening reaction of RhBHA moieties and lead to the macroscopic colorimetric changes (Figures 2 and 4).

To further investigate the fluorometric transition of micellar solution of P(St-*co*-NBDAE)$_{20}$-*b*-P(NIPAM-*co*-RhBHA)$_{54}$ occurred upon addition of Cu^{2+} ions, fluorometric titration experiments were conducted upon addition of Cu^{2+} ions and the results are shown in Figure 5. It was found that the decrease of NBDAE emission band at ∼518 nm are clearly evident accompanied by the increase of Cu^{2+} concentrations. On the other hand, it is quite surprising that the emission bands of acyclic RhBHA is not discernible, suggesting that acyclic RhBHA induced by Cu^{2+} ions is nonemissive, probably due to the quenching effects of Cu^{2+} ions (d−d electron paramagnetism).[71] This results also agrees with the previous report of the Cu^{2+}-sensing behavior of PEO-*b*-P(NIPAM-*co*-RhBHA) double hydrophilic block copolymers.[60] Moreover, preliminary experiments revealed that Cu^{2+} ions can not quench the fluorescence emission of NBDAE monomer and micelles of P(St-*co*-NBDAE)$_{20}$-*b*-P(NIPAM-*co*-RhBHA)$_{54}$. Thus, the decrease of NBDAE emission bands for the micellar solution of P(St-*co*-NBDAE)$_{20}$-*b*-P(NIPAM-*co*-RhBHA)$_{54}$ should be ascribed to the FRET process between NBDAE moieties and acyclic RhBHA moieties induced by Cu^{2+} ions. This is further confirmed by the excellent spectral overlap between NBDAE emission and the absorption of acyclic RhBHA induced by Cu^{2+} ions (Figure S6 (Supporting Information)). As shown in Figure 5b, the fluorescence emission intensity (I_{518}) ascribing to NBDAE dramatically decreased upon the addition of Cu^{2+} ions and stabilized out in the presence of >∼1.0 equiv of Cu^{2+} ions. If we define the detection limit as the Cu^{2+} concentration at which a 10% fluorescence intensity decrease (I_{518}) can be detected by utilizing the 0.05 g/L micellar solution, the Cu^{2+} detection limit was determined to be 4.3 ppb (Figure 5c). On the basis of the above results, we have established that micellar solution of P(St-*co*-NBDAE)$_{20}$-*b*-P(NIPAM-*co*-RhBHA)$_{54}$ amphiphilic diblock copolymer at 25 °C can effectively act as colorimetric and ratiometric fluorometric probes for Hg^{2+} ions, accompanied by the almost colorless to pink and green-to-orange transitions, respectively, and the Hg^{2+} ion detection limit of ∼14.8 ppb can be reached. Moreover, the diblock copolymer micelles can also server as fluorometric Cu^{2+} probes with the detection limit down to ∼4.3 ppb.

Within P(St-*co*-NBDAE)$_{20}$-*b*-P(NIPAM-*co*-RhBHA)$_{54}$ micelles, the NBDAE moieties and fluorescence emission off/on switchable RHBHA moieties are located in micellar cores and coronas, respectively (Scheme 1). Thus, the thermo-induced collapse of P(NIPAM-*co*-RhBHA) coronas can be further utilized to tune the spatial proximity between FRET donor and acceptor moieties.[72−76] We then examined the fluorometric responses of P(St-*co*-NBDAE)$_{20}$-*b*-P(NIPAM-*co*-RhBHA)$_{54}$ micelles in the presence of ∼1.0 equiv. Hg^{2+} ions when the detection temperature varies in the range of 25−40 °C. From the emission spectrum, we can obviously observe two well-resolved emission peaks respectively centered at ∼518 and 580 nm, and the latter can be ascribed to RhBHA moieties partially existing in the acyclic form induced by the addition of ∼1.0 equiv. Hg^{2+} ions (Figure 6). With the increase of temperatures, it was found that the NBDAE emission band at

~518 nm decreases, accompanied by the intensity increase of acyclic RhBHA emission band. The fluorescence intensity ratio (I_{585}/I_{518}) increased from 0.56 (at 25 °C) to 2.2 (at 40 °C). Moreover, when the temperature was cycled between 25 and 40 °C, we can observe from Figure 6c that the intensity ratio (I_{585}/I_{518}) can repeatedly switch between ~0.56 and 2.2. The above results suggested that P(St-*co*-NBDAE)$_{20}$-*b*-P(NIPAM-*co*-RhBHA)$_{54}$ micelles can also serve as ratiometric fluorescent thermal sensors.

Three factors might contribute to the increase of acyclic RhBHA bands upon increasing temperatures in the presence of 1.0 equiv of Hg^{2+} ions: (1) the possible generation of more acyclic RhBHA species at elevated temperatures; (2) enhanced RhBHA emission due to the more hydrophobic microenvironment of PNIPAM coronas at elevated temperatures; (3) enhanced FRET efficiency due to thermo-induced collapse of PNIPAM coronas (Scheme 1). To elucidate the respective effects of the above three factors, the following control experiments were conducted. First, PS$_{20}$-*b*-P(DMA-*co*-RhBHA)$_{57}$ with the RhBHA dye content in the hydrophilic block comparable to P(St-*co*-NBDAE)$_{20}$-*b*-P(NIPAM-*co*-RhBHA)$_{54}$ was synthesized, where DMA is *N*,*N*-dimethylacrylamide. The corona of PS$_{20}$-*b*-P(DMA-*co*-RhBHA)$_{57}$ is permanently hydrophilic. Results shown in Figure S12 (Supporting Information) revealed that both the fluorescence emission (excited at 560 nm) and absorbance of acyclic RhBHA moieties in the presence of 1.0 equiv. Hg^{2+} ions exhibited ~10% enhancement at 40 °C compared to that at 25 °C, which should be ascribed to the possible generation of more acyclic RhBHA moieties at elevated temperatures. Second, we also synthesized PS$_{20}$-*b*-P(NIPAM-*co*-RhBHA)$_{55}$, which contains no NBDAE moieties in the PS block and comparable RhBHA dye content in the PNIPAM block. Fluorescence measurements of the micellar solution of PS$_{20}$-*b*-P(NIPAM-*co*-RhBHA)$_{55}$ upon addition of 1.0 equiv. Hg^{2+} ions revealed ~30% enhancement in emission intensity at 40 °C compared to that at 25 °C (Figure S13 (Supporting Information)). It should be noted that the ~30% enhancement should be ascribed to contributions from both the generation of more acyclic species and the more hydrophobic microenvironment of PNIPAM coronas at elevated temperatures.[60,92,93] Finally, we also synthesized P(St-*co*-NBDAE)$_{20}$-*b*-PNIPAM$_{56}$ which contains no RhBHA species in the PNIPAM block. It was found that the NBDAE emission (excited at 470 nm) of P(St-*co*-NBDAE)$_{20}$-*b*-PNIPAM$_{56}$ micelles remains essentially constant upon heating from 25 to 40 °C (Figure S14 (Supporting Information)), suggesting that the quantum yield of NBDAE located within hydrophobic PS cores is not sensitive to external temperature changes.

For the micellar solution of P(St-*co*-NBDAE)$_{20}$-*b*-P(NIPAM-*co*-RhBHA)$_{54}$ in the presence of 1.0 equiv of Hg^{2+} ions, we can observe from Figure 6 that the intensity of NBDAE emission band decreased ~54.5% ($1 - I/I_0$ at 518 nm) and the intensity of RhBHA band exhibited ~70% enhancement (I/I_0 at 585 nm). The prominent decrease of NBDAE emission intensity at elevated temperatures can be solely ascribed to the enhancement of FRET efficiencies due to the corona collapse-induced closer proximity between FRET donor and acceptors at elevated temperatures. This also correlates quite well with the temperature-dependent optical transmittance results (Figure S4 (Supporting Information)) and LLS results (Figure S5 (Supporting Information)). Moreover, the contribution of enhanced FRET process can be further verified by the 70% enhancement of acyclic RhBHA band, as compared to the ~30% increase for PS$_{20}$-*b*-P(NIPAM-*co*-RhBHA)$_{55}$ micelles in the same temperature range. Thus, we can conclude that the above-mentioned three factors can cooperatively contribute to the enhanced acyclic RhBHA emission at elevated temperatures (Figure 6).

Preliminary fluorescence imaging of Hg^{2+} ions within HeLa cells was further conducted. As shown in Figure S15 (Supporting Information), HeLa cells cultured in the presence of 0.1 g/L micellar solution of P(St-*co*-NBDAE)$_{20}$-*b*-P(NIPAM-*co*-RhBHA)$_{54}$ exhibit green emission ascribed to NBDAE moieties (Figure S15a (Supporting Information)) in the absence of Hg^{2+} ions. However, upon addition of 5.0 equiv. Hg^{2+} ions and incubation for 30 min, the fluorescence emission dramatically changed from green to red under inverted fluorescence microscopy (Figure S15b (Supporting Information)), indicating that P(St-*co*-NBDAE)$_{20}$-*b*-P(NIPAM-*co*-RhBHA)$_{54}$ micelles can effectively enter into living cells for the imaging of Hg^{2+} ions. Because of that Hg^{2+} ions can selectively switch on the FRET process between FRET donor and potential FRET acceptor, the presented two-color imaging of Hg^{2+} ions is expected to considerably enhance the temporal and spatial resolution of Hg^{2+} ions within living cells.

In the previous work concerning PEO$_{113}$-*b*-P(NIPAM-*co*-RhBHA)$_{69}$-based fluorescent sensor for Hg^{2+} ions,[60] the detection limit of Hg^{2+} ions is ~3.5 ppb at 25 °C. Note that this system is based on changes in fluorescence intensities of a single emission band. Although for P(St-*co*-NBDAE)$_{20}$-*b*-P(NIPAM-*co*-RhBHA)$_{54}$ micelles, the Hg^{2+} detection limit is 14.8 ppb at 25 °C, the characteristics of ratiometric fluorescence sensing can offer extra advantages such as the effective elimination of background interference, internal self-calibration, and the capability of two-color imaging (as indicated by the cell imaging results shown in Figure S15 (Supporting Information)). Most importantly, P(St-*co*-NBDAE)$_{20}$-*b*-P(NIPAM-*co*-RhBHA)$_{54}$ micelles are also capable of highly efficient fluorescent Cu^{2+} sensing with the detection down to ~4.3 ppb; whereas this feature is not available for PEO$_{113}$-*b*-P(NIPAM-*co*-RhBHA)$_{69}$ sensing system. Finally, the ratiometric fluorescent detection sensitivity for Hg^{2+} ions (especially in the medium concentration range of 0.5−2.0 ppm) can be modulated by changing relative block lengths (as shown in Figure S11 (Supporting Information)) and the detection limit can be tuned by lowering micellar concentrations.

It should be noted that the nonfluorescent RhBHA moieties in the spirolactam form can also undergo reversible chemical transformation to highly fluorescent acyclic species in acidic media, as reported previously.[60] Thus, we expect that the amphiphilic block copolymer micelles can also serve as ratiometric fluorescent pH probes (Scheme 1). Above ~pH 6, the micellar solution of P(St-*co*-NBDAE)$_{20}$-*b*-P(NIPAM-*co*-RhBHA)$_{54}$ only possess green emission band of NBDAE moieties, suggesting that the RhBHA moieties are in the spirolactam form (Figure 7). In the pH range of 3−6 at 25 °C, we can clearly observe the decrease of NBDAE emission intensity at ~518 nm and the prominent increase of acyclic RhBHA emission intensity at ~580 nm, indicating the FRET process between NBDAE and RhBHA has been effectively switched on under acidic conditions. As shown in Figure 7b, the fluorescence emission intensity ratios (I_{585}/I_{518}) dramatically increased from 0.43 (pH 9) to 2.01 (pH 3) at 25 °C, i.e., ~4.7-fold increase. Intriguingly, upon heating the micellar solution to 40 °C, which is higher than the LCST of thermoresponsive P(NIPAM-*co*-RhBHA) coronas (Figure S4 (Supporting Information)), the fluorescence intensity

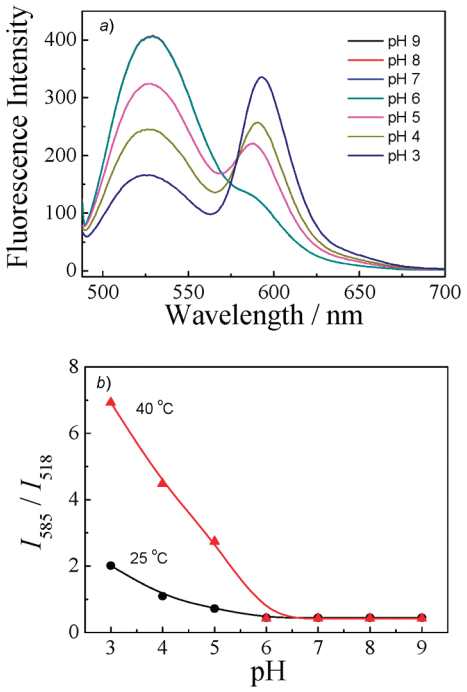

Figure 7. (a) Fluorescence emission spectra and (b) fluorescence intensity ratio changes of 0.05 g/L micellar solution of P(St-*co*-NBDAE)$_{20}$-*b*-P(NIPAM-*co*-RhBHA)$_{54}$ at 25 °C in the pH range of 3−9, and the fluorescence emission intensity ratio changes at 40 °C recorded in the same pH range ([RhBHA] = 1.57 μM; λ_{ex} = 470 nm; slit width, Ex. 5 nm, Em. 5 nm).

ratio (I_{585}/I_{518}) further exhibits ∼3.5-fold increase at pH 3 (Figure 7b). In the pH range of 3−9, ∼16.3-fold increase in the fluorescence intensity ratio can be determined at 40 °C, which is much larger that that at 25 °C (∼4.7-fold). Thus, the reported diblock copolymer micelles possess ratiometric fluorometric pH-sensing capability with considerably enhanced sensitivities at temperatures above the thermal phase transition temperature of thermoresponsive P(NIPAM-*co*-RhBHA) coronas, as compared to that at 25 °C.

CONCLUSIONS

In summary, FRET pair consisting of 4-(2-acryloyloxyethylamino)-7-nitro-2,1,3-benzoxadiazole (NBDAE) donor and rhodamine B-based potential acceptor (RhBHA) in the spirolactam form with pH and Hg^{2+}- (Cu^{2+}-) reactive characteristics were respectively copolymerized into the hydrophobic PS and thermoresponsive PNIPAM block of P(St-*co*-NBDAE)-*b*-P(NIPAM-*co*-RhBHA) amphiphilic diblock copolymers. Self-assembled micelles of the as-synthesized amphiphilic diblock can serve as multifunctional ratiometric fluorescent chemosensors for metal ions (Hg^{2+} and Cu^{2+}), pH, and temperatures due to the Hg^{2+}- and pH-reactiveness of RhBHA moieties within the thermoresponsive coronas. On the other hand, Cu^{2+} ions can quantitatively induce the ring-opening of RhBHA moieties and afford nonfluorescent species with broad absorption band, which can effectively quench the NBDAE emission via the FRET mechanism. Therefore, amphiphilic diblock copolymer micelles can also quantitatively report the presence of Cu^{2+} ions based on the relative changes of NBDAE emission intensities. Most importantly, the spatial distance between the FRET pair can be facilely tuned via thermo-induced collapse of PNIPAM micellar coronas, which dramatically increased the FRET efficiency and enhanced pH detection sensitivity. Compared to small molecule-based fluorometric metal ion probes, the reported amphiphilic diblock copolymer micelles-based sensing system bestows prominent advantages such as water-solubility, structural stability, multifunctional integration, tunable detection sensitivity, and the ability of further functionalization for targeted delivery and controlled release. Further work toward this direction, including the development of amphiphilic diblock copolymer micelles-based living cell imaging and sensing devices, is currently underway.

ASSOCIATED CONTENT

Supporting Information. Summary of structural parameters, ^{1}H NMR spectra, THF GPC traces, determination of critical micellization concentration, temperature-dependence of optical transmittance, hydrodynamic radius distributions, scattering vector dependence of Rayleigh ratio, normalized fluorescence emission spectrum, time-dependent changes of fluorescence intensity ratios, UV-Vis absorbance spectra and absorbance intensity changes, fluorescence emission spectra and fluorescence intensity changes, fluorescence intensity ratio changes, normalized fluorescence emission and absorption spectra, and fluorescent images of HeLa cells incubated with micellar solutions This material is available free of charge via the Internet at http://pubs.acs.org.

AUTHOR INFORMATION

Corresponding Author
*E-mail: sliu@ustc.edu.cn.

ACKNOWLEDGMENT

The financial support from the National Natural Scientific Foundation of China (NNSFC) Project (51033005, 20874092, 91027026, and 21090354), Fundamental Research Funds for the Central Universities, and Specialized Research Fund for the Doctoral Program of Higher Education (SRFDP) is gratefully acknowledged.

REFERENCES

(1) Boening, D. W. *Chemosphere* **2000**, *40*, 1335–1351.
(2) Benoit, J. M.; Fitzgerald, W. F.; Damman, A. W. H. *Environ. Res.* **1998**, *78*, 118–133.
(3) Yang, Y. K.; Yook, K. J.; Tae, J. *J. Am. Chem. Soc.* **2005**, *127*, 16760–16761.
(4) Wu, J. S.; Hwang, I. C.; Kim, K. S.; Kim, J. S. *Org. Lett.* **2007**, *9*, 907–910.
(5) Wu, D. Y.; Huang, W.; Duan, C. Y.; Lin, Z. H.; Meng, Q. J. *Inorg. Chem.* **2007**, *46*, 1538–1540.
(6) Wang, J. B.; Qian, X. H. *Org. Lett.* **2006**, *8*, 3721–3724.
(7) Ros-Lis, J. V.; Marcos, M. D.; Martinez-Manez, R.; Rurack, K.; Soto, J. *Angew. Chem., Int. Ed.* **2005**, *44*, 4405–4407.
(8) Yoon, S.; Miller, E. W.; He, Q.; Do, P. H.; Chang, C. J. *Angew. Chem., Int. Ed.* **2007**, *46*, 6658–6661.
(9) Rurack, K.; Kollmannsberger, M.; Resch-Genger, U.; Daub, J. *J. Am. Chem. Soc.* **2000**, *122*, 968–969.
(10) Ko, S. K.; Yang, Y. K.; Tae, J.; Shin, I. *J. Am. Chem. Soc.* **2006**, *128*, 14150–14155.
(11) Yoon, S.; Albers, A. E.; Wong, A. P.; Chang, C. J. *J. Am. Chem. Soc.* **2005**, *127*, 16030–16031.
(12) Nolan, E. M.; Racine, M. E.; Lippard, S. J. *Inorg. Chem.* **2006**, *45*, 2742–2749.

(13) Kim, S. H.; Kim, J. S.; Park, S. M.; Chang, S. K. *Org. Lett.* **2006**, *8*, 371–374.
(14) Caballero, A.; Martinez, R.; Lloveras, V.; Ratera, I.; Vidal-Gancedo, J.; Wurst, K.; Tarraga, A.; Molina, P.; Veciana, J. *J. Am. Chem. Soc.* **2005**, *127*, 15666–15667.
(15) Liu, B.; Tian, H. *Chem. Commun.* **2005**, 3156–3158.
(16) Nolan, E. M.; Lippard, S. J. *J. Am. Chem. Soc.* **2003**, *125*, 14270–14271.
(17) Kim, J. S.; Choi, M. G.; Song, K. C.; No, K. T.; Ahn, S.; Chang, S. K. *Org. Lett.* **2007**, *9*, 1129–1132.
(18) Shiraishi, Y.; Maehara, H.; Ishizumi, K.; Hirai, T. *Org. Lett.* **2007**, *9*, 3125–3128.
(19) Chen, X. Q.; Nam, S. W.; Jou, M. J.; Kim, Y.; Kim, S. J.; Park, S.; Yoon, J. *Org. Lett.* **2008**, *10*, 5235–5238.
(20) Brummer, O.; La Clair, J. J.; Janda, K. D. *Org. Lett.* **1999**, *1*, 415–418.
(21) Lee, M. H.; Cho, B. K.; Yoon, J.; Kim, J. S. *Org. Lett.* **2007**, *9*, 4515–4518.
(22) Zhang, G. X.; Zhang, D. Q.; Yin, S. W.; Yang, X. D.; Shuai, Z.; Zhu, D. B. *Chem. Commun.* **2005**, 2161–2163.
(23) Wang, J. B.; Qian, X. H. *Chem. Commun.* **2006**, 109–111.
(24) Lee, M. H.; Wu, J. S.; Lee, J. W.; Jung, J. H.; Kim, J. S. *Org. Lett.* **2007**, *9*, 2501–2504.
(25) Guo, X. F.; Qian, X. H.; Jia, L. H. *J. Am. Chem. Soc.* **2004**, *126*, 2272–2273.
(26) Shi, W.; Ma, H. M. *Chem. Commun.* **2008**, 1856–1858.
(27) Zheng, H.; Qian, Z. H.; Xu, L.; Yuan, F. F.; Lan, L. D.; Xu, J. G. *Org. Lett.* **2006**, *8*, 859–861.
(28) Ros-Lis, J. V.; Martinez-Manez, R.; Rurack, K.; Sancenon, F.; Soto, J.; Spieles, M. *Inorg. Chem.* **2004**, *43*, 5183–5185.
(29) Suresh, M.; Shrivastav, A.; Mishra, S.; Suresh, E.; Das, A. *Org. Lett.* **2008**, *10*, 3013–3016.
(30) Wu, D. Y.; Huang, W.; Lin, Z. H.; Duan, C. Y.; He, C.; Wu, S.; Wang, D. H. *Inorg. Chem.* **2008**, *47*, 7190–7201.
(31) Hu, Z. Q.; Lin, C. S.; Wang, X. M.; Ding, L.; Cui, C. L.; Liu, S. F.; Lu, H. Y. *Chem. Commun.* **2010**, *46*, 3765–3767.
(32) Zhang, X. L.; Xiao, Y.; Qian, X. H. *Angew. Chem., Int. Ed.* **2008**, *47*, 8025–8029.
(33) Ou, S. J.; Lin, Z. H.; Duan, C. Y.; Zhang, H. T.; Bai, Z. P. *Chem. Commun.* **2006**, 4392–4394.
(34) Lv, J.; Ouyang, C.; Yin, X. D.; Zheng, H. Y.; Zuo, Z. C.; Xu, J. L.; Liu, H. B.; Li, Y. L. *Macromol. Rapid Commun.* **2008**, *29*, 1588–1592.
(35) Tang, Y. L.; He, F.; Yu, M. H.; Feng, F. D.; An, L. L.; Sun, H.; Wang, S.; Li, Y. L.; Zhu, D. B. *Macromol. Rapid Commun.* **2006**, *27*, 389–392.
(36) Kim, I. B.; Bunz, U. H. F. *J. Am. Chem. Soc.* **2006**, *128*, 2818–2819.
(37) Liu, S. J.; Fang, C.; Zhao, Q.; Fan, Q. L.; Huang, W. *Macromol. Rapid Commun.* **2008**, *29*, 1212–1215.
(38) Qin, C. J.; Wu, X. F.; Gao, B. X.; Tong, H.; Wang, L. X. *Macromolecules* **2009**, *42*, 5427–5429.
(39) Fang, Z.; Pu, K. Y.; Liu, B. *Macromolecules* **2008**, *41*, 8380–8387.
(40) Kim, I. B.; Phillips, R.; Bunz, U. H. F. *Macromolecules* **2007**, *40*, 814–817.
(41) Wang, Y. S.; Liu, B. *Macromol. Rapid Commun.* **2009**, *30*, 498–503.
(42) Lee, S. J.; Lee, J. E.; Seo, J.; Jeong, I. Y.; Lee, S. S.; Jung, J. H. *Adv. Funct. Mater.* **2007**, *17*, 3441–3446.
(43) Delgado-Pinar, E.; Montoya, N.; Galiana, M.; Albelda, M. T.; Frias, J. C.; Jimenez, H. R.; Garcia-Espana, E.; Alarcon, J. *New J. Chem.* **2010**, *34*, 567–570.
(44) Wang, C.; Tao, S. Y.; Wei, W.; Meng, C. G.; Liu, F. Y.; Han, M. *J. Mater. Chem.* **2010**, *20*, 4635–4641.
(45) Freeman, R.; Finder, T.; Willner, I. *Angew. Chem., Int. Ed.* **2009**, *48*, 7818–7821.
(46) Han, B. Y.; Yuan, J. P.; Wang, E. K. *Anal. Chem.* **2009**, *81*, 5569–5573.
(47) Huang, C. C.; Chang, H. T. *Anal. Chem.* **2006**, *78*, 8332–8338.
(48) Lee, J. S.; Han, M. S.; Mirkin, C. A. *Angew. Chem., Int. Ed.* **2007**, *46*, 4093–4096.
(49) Liu, C. W.; Huang, C. C.; Chang, H. T. *Langmuir* **2008**, *24*, 8346–8350.
(50) He, S. J.; Li, D.; Zhu, C. F.; Song, S. P.; Wang, L. H.; Long, Y. T.; Fan, C. H. *Chem. Commun.* **2008**, 4885–4887.
(51) Huang, C. C.; Yang, Z.; Lee, K. H.; Chang, H. T. *Angew. Chem., Int. Ed.* **2007**, *46*, 6824–6828.
(52) Xie, J. P.; Zheng, Y. G.; Ying, J. Y. *Chem. Commun.* **2010**, *46*, 961–963.
(53) Wang, Z. D.; Lee, J. H.; Lu, Y. *Chem. Commun* **2008**, 6005–6007.
(54) Wang, J.; Liu, B. *Chem. Commun.* **2008**, 4759–4761.
(55) Ma, L. J.; Li, Y.; Li, L.; Sun, J.; Tian, C. J.; Wu, Y. Q. *Chem. Commun.* **2008**, 6345–6347.
(56) Zhang, X. R.; Li, Y.; Su, H. R.; Zhang, S. S. *Biosens. Bioelectron.* **2010**, *25*, 1338–1343.
(57) Matsushita, M.; Meijler, M. M.; Wirsching, P.; Lerner, R. A.; Janda, K. D. *Org. Lett.* **2005**, *7*, 4943–4946.
(58) Miyake, Y.; Togashi, H.; Tashiro, M.; Yamaguchi, H.; Oda, S.; Kudo, M.; Tanaka, Y.; Kondo, Y.; Sawa, R.; Fujimoto, T.; Machinami, T.; Ono, A. *J. Am. Chem. Soc.* **2006**, *128*, 2172–2173.
(59) Dave, N.; Chan, M. Y.; Huang, P. J. J.; Smith, B. D.; Liu, J. W. *J. Am. Chem. Soc.* **2010**, *132*, 12668–12673.
(60) Hu, J. M.; Li, C. H.; Liu, S. Y. *Langmuir* **2010**, *26*, 724–729.
(61) Li, C. H.; Liu, S. Y. *J. Mater. Chem.* **2010**, *20*, 10716–10723.
(62) Sasaki, D. Y.; Padilla, B. E. *Chem. Commun.* **1998**, 1581–1582.
(63) Zhang, X. B.; Guo, C. C.; Li, Z. Z.; Shen, G. L.; Yu, R. Q. *Anal. Chem.* **2002**, *74*, 821–825.
(64) Nolan, E. M.; Lippard, S. J. *Chem. Rev.* **2008**, *108*, 3443–3480.
(65) Valecur, B. *Molecular Fluorescence: Principles and Applications*: Wiley-VCH: New York, 2002.
(66) Lakowicz, J. R. *Principles of Fluorescence Spectroscopy*: Plenum: New York, 1999.
(67) Nolan, E. M.; Lippard, S. J. *J. Am. Chem. Soc.* **2007**, *129*, 5910–5918.
(68) Nolan, E. M.; Lippard, S. J. *J. Mater. Chem.* **2005**, *15*, 2778–2783.
(69) Fang, G.; Xu, M. Y.; Zeng, F.; Wu, S. Z. *Langmuir* **2010**, *26*, 17764–17771.
(70) Hu, J. M.; Liu, S. Y. *Macromolecules* **2010**, *43*, 8315–8330.
(71) Kim, H. N.; Guo, Z. Q.; Zhu, W. H.; Yoon, J.; Tian, H. *Chem. Soc. Rev.* **2011**, *40*, 79–93.
(72) Liu, T.; Hu, J. M.; Yin, J.; Zhang, Y. F.; Li, C. H.; Liu, S. Y. *Chem. Mater.* **2009**, *21*, 3439–3446.
(73) Wu, T.; Zou, G.; Hu, J. M.; Liu, S. Y. *Chem. Mater.* **2009**, *21*, 3788–3798.
(74) Wan, X. J.; Wang, D.; Liu, S. Y. *Langmuir* **2010**, *26*, 15574–15579.
(75) Yin, J.; Guan, X. F.; Wang, D.; Liu, S. Y. *Langmuir* **2009**, *25*, 11367–11374.
(76) Yin, J.; Li, C. H.; Wang, D.; Liu, S. Y. *J. Phys. Chem. B* **2010**, *114*, 12213–12220.
(77) Liu, T.; Liu, S. Y. *Anal. Chem.* **2011**, *83*, 2775–2785.
(78) Wan, X. J.; Liu, T.; Liu, S. Y. *Langmuir* **2011**, 4082–4090.
(79) Wang, D.; Liu, T.; Yin, J.; Liu, S. Y. *Macromolecules* **2011**, *44*, 2282–2290.
(80) Hu, J. M.; Li, C. H.; Cui, Y.; Liu, S. Y. *Macromol. Rapid Commun.* **2011**, *32*, 610–615.
(81) Li, C. H.; Hu, J. M.; Liu, T.; Liu, S. Y. *Macromolecules* **2011**, *44*, 429–431.
(82) Yin, J.; Hu, H. B.; Wu, Y. H.; Liu, S. Y. *Polym. Chem.* **2011**, *2*, 363–371.
(83) Li, C. H.; Zhang, Y. X.; Hu, J. M.; Cheng, J. J.; Liu, S. Y. *Angew. Chem., Int. Ed.* **2010**, *49*, 5120–5124.
(84) Uchiyama, S.; Matsumura, Y.; de Silva, A. P.; Iwai, K. *Anal. Chem.* **2003**, *75*, 5926–5935.

(85) Lai, J. T.; Filla, D.; Shea, R. *Macromolecules* **2002**, *35*, 6754–6756.
(86) Xu, J.; Luo, S. Z.; Shi, W. F.; Liu, S. Y. *Langmuir* **2006**, *22*, 989–997.
(87) Luo, S. Z.; Xu, J.; Zhu, Z. Y.; Wu, C.; Liu, S. Y. *J. Phys. Chem. B* **2006**, *110*, 9132–9139.
(88) Wu, T.; Zhang, Y. F.; Wang, X. F.; Liu, S. Y. *Chem. Mater.* **2008**, *20*, 101–109.
(89) Ma, B. L.; Wu, S. Z.; Zeng, F.; Luo, Y. L.; Zhao, J. Q.; Tong, Z. *Nanotechnology* **2010**, *21*, 195501.
(90) Ma, C.; Zeng, F.; Huang, L.; Wu, S. *J. Phys. Chem. B* **2011**, *115*, 874–882.
(91) Chae, M. Y.; Czarnik, A. W. *J. Am. Chem. Soc.* **1992**, *114*, 9704–9705.
(92) Shiraishi, Y.; Miyamoto, R.; Hirai, T. *J. Photochem. Photobiol. A: Chem.* **2008**, *200*, 432–437.
(93) Shiraishi, Y.; Miyamoto, R.; Zhang, X.; Hirai, T. *Org. Lett.* **2007**, *9*, 3921–3924.